ELSEVIER

International Journal of Mass Spectrometry 212 (2001) 273–286

International Journal of Mass Spectrometry

www.elsevier.com/locate/ijms

A new time-of-flight gating method for analyzing kinetic energy release in Coulomb exploded clusters: application to water clusters

Eric S. Wisniewski[a], Jason R. Stairs[a], A. Welford Castleman, Jr.[b,*]

[a]*Department of Chemistry, The Pennsylvania State University, University Park, Pennsylvania 16802*

[b]*Departments of Chemistry and Physics, The Pennsylvania State University, University Park, Pennsylvania 16802*

Received 19 April 2001; accepted 7 June 2001

Abstract

A new method is presented for the analysis of high energy multicharged cations produced by Coulomb explosion in a time-of-flight mass spectrometer. The technique employs energy gating through a manipulation of electric potentials in the Wiley–McLaren lens assembly, and the use of a reflecting electric field. Water clusters of sizes up to about 20 molecules were irradiated with femtosecond laser pulses to generate protons and multicharged oxygen atoms. Protons with energies in excess of 3 kV are reported as well as O^{4+} ions with energies in excess of 13 kV. (Int J Mass Spectrom 212 (2001) 273–286) © 2001 Elsevier Science B.V.

Keywords: Cluster; Coulomb explosion; Time-of-flight; Water; Femtosecond

1. Introduction

Investigations into the behavior of molecular species and clusters subjected to the intense optical fields provided by amplified femtosecond laser systems are being pursued in a number of laboratories [1–6]. Femtosecond laser pulses of short duration and sufficiently high power are employed, removing many electrons of a molecular cluster in ~20 fs [7]. Since the timescale of electron removal is of such short duration, the heavy nuclei acquire their high positive charge before there is sufficient time for substantial nuclear rearrangement which generally occurs on the picosecond time scale [8,9]. The large Coulomb potential arising from atoms with high charge states generated in close proximity to one another converts to kinetic energy as the like charges repel each other. This intense fragmentation has been termed Coulomb explosion and has been shown to yield charged particles with enormous magnitudes of kinetic energy. The finding of great enhancement in the process upon the irradiation of clusters compared to individual molecules or solids have generated great interest in the scientific community and a number of experimental and theoretical papers have been published concerning this phenomenon [10,11]. A particularly interesting and useful application has led to the ability to use Coulomb explosion to directly study intermediates in fast reactions [12].

Several mechanisms have been proposed to ac-

* Corresponding author. E-mail: awc@psu.edu

This paper is submitted in honor of Professor R. Graham Cooks on the occasion of his 60th birthday.

PII S1387-3806(01)00479-1

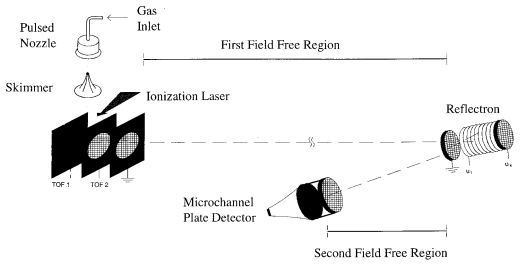

Fig. 1. Pictured is an illustration of the reflectron time-of-flight mass spectrometer. The reflectron is situated at an angle to redirect ions toward the detector. For the studies presented here, the reflectron was operated in hard reflection mode where a potential was applied to u_t only.

count for the experimental and theoretical findings associated with Coulomb explosion. These are the coherent electron motion model, the ionization ignition model, the charge-resonance-enhanced ionization (CREI) mechanism, the dynamic CREI, and the nonvertical ionization mechanism [13–17]. Earlier findings in our laboratories suggest the dynamic CREI mechanism most closely accounts for experimental evidence for small and intermediate clusters [18]. The initial CREI model proposes that the electric field of the laser pulse promotes electrons above the ground state, suppresses tunneling, and lowers the external barrier to ionization when in resonance with particular internuclear separations [16]. The dynamic CREI mechanism takes further account of the transient behavior of both the laser pulse and the spatially expanding cluster system, and explains the production of high charge states as being due to progressive collective electron excitation as the laser pulse continually propagates [9,16].

The ions generated from a Coulomb explosion event often yield a signature peak shape when detected in a time-of-flight mass spectrometer (TOFMS) such as one shown schematically in Fig. 1. In a long drift field, well-collimated TOFMS, only those ions accelerated along the axis of the machine become detected. This apparatus arrangement is such that when a cluster or molecule undergoes Coulomb explosion, only those fragments ejected along the axis of the mass spectrometer are detected, with all others being lost. Fig. 2 shows a typical signature peak which is observed from a Coulomb explosion event in ammonia clusters. An exploded cluster has forward- and backward-ejected fragments. Those fragments directed forward proceed toward the detector with a distribution of energies and are recorded as a hump in the mass spectrum. As indicated schematically in Fig. 3, the fragments that are directed backwards are turned around by the field produced by time-of-flight $(TOF)_1$, and with judicious selection of electrostatic potentials, some compensation for the energy distribution can be attained so that those ions are forced toward the detector and arrive as a narrow packet. This accounts for the general nature of the peak shapes given in Fig. 2.

Experimental values of the kinetic energy release (KER) from a Coulomb explosion event have been determined in our laboratories in two independent ways, the peak analysis method and the reflectron cut-off method [3,10]. The first takes into account the signature peak shape of the Coulomb explosion. By measuring the time between the forward- and backward-ejected packets, the kinetic energy release can be determined as described below. The second method takes advantage of the reflectron shown in Fig. 1, which can serve as an energy analyzer. Initially, the reflectron is set at a voltage much higher than the birth potential (the potential at which all ions are born between the time-of-flight grids). Forward- and backward-ejected ions each possess more energy than that supplied by the birth potential. As the reflectron voltage is systematically reduced, those ions with energy higher than that of the reflectron continue on a straight path and are not turned toward the detector. Determining electric potentials at which charged species are sequentially lost leads to a determination of the birth potential of those that do not undergo Coulomb explosion, and the kinetic energy distribution of those that do.

The cutoff method provides a good estimate of the kinetic energy release in a Coulomb explosion event by removing the high-energy species first. However, this method is limited by practical considerations concerning the maximum voltage, which can be applied to the reflectron. Hence, depending on the magnitude of kinetic energy acquired in the Coulomb explosion process, limitations of the apparatus may

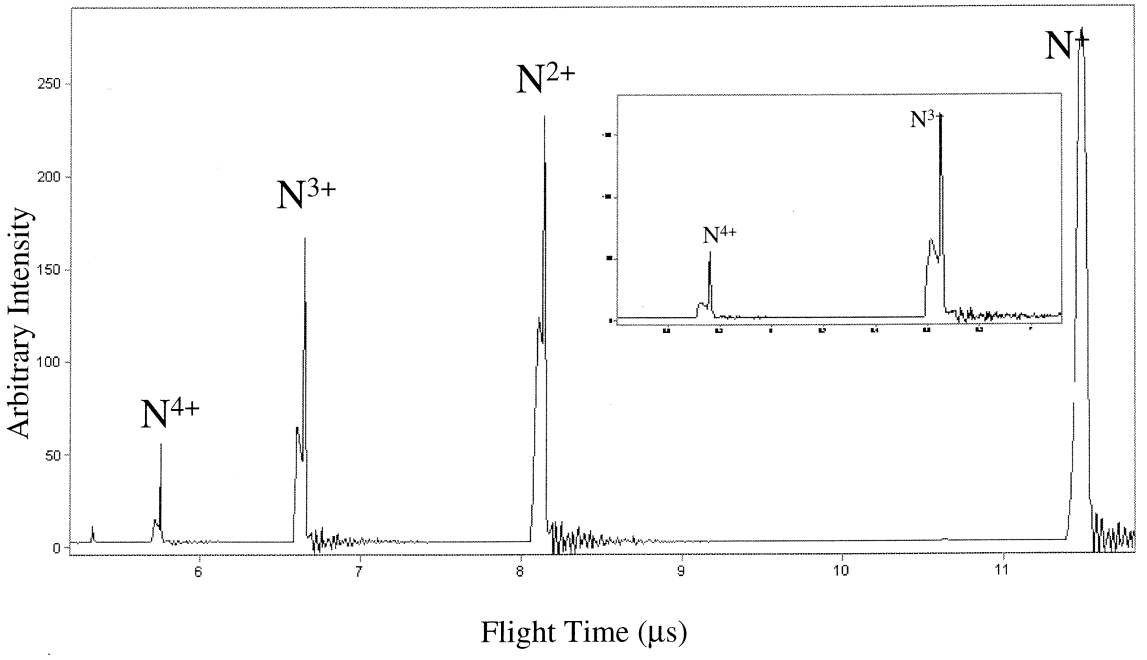

Fig. 2. Signature peak splitting from a Coulomb explosion event. Here, multicharged nitrogen results from the Coulomb explosion of ammonia clusters.

impede the ability to characterize the full kinetic energy distribution. This is illustrated in Fig. 4. Species with energy higher than the maximum voltage of the reflectron will not be detected as they will proceed in a linear trajectory and will not be turned toward the detector as required for imaging by the arrangement shown in Fig. 1 [5,19].

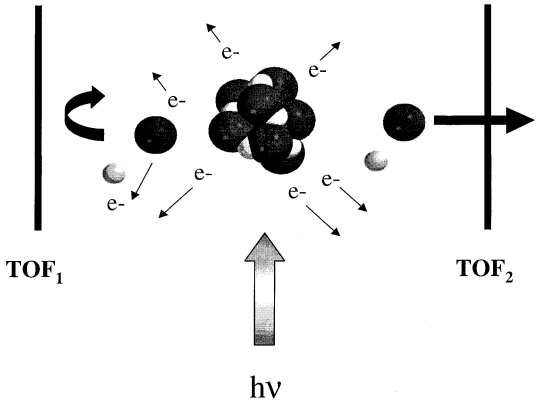

Fig. 3. Schematic representation of forward- and backward-ejected fragments from Coulomb explosion. Fragments fired forward arrive at the detector in a broad hump while fragments fired backward are turned around by the field applied to TOF_1 and arrive at the detector after being focused.

Presented here is a new method that enables detecting even very large well-defined KER ranges by quantitatively lowering the energy of the highly energetic species so that they may be detected. By gating certain energy ranges, the total kinetic energy distribution can be obtained up to the limit of the mass spectrometer imposed by the potentials, which can be applied to the various electrical lenses. However, the gating method considerably extends the magnitude of the kinetic energies which can be studied compared to the more conventional techniques.

2. Experimental

Water clusters were generated via supersonic expansion of room-temperature water vapor seeded in helium at a pressure between 1.7 and 2.4 bar. The molecular beam produced in this fashion was

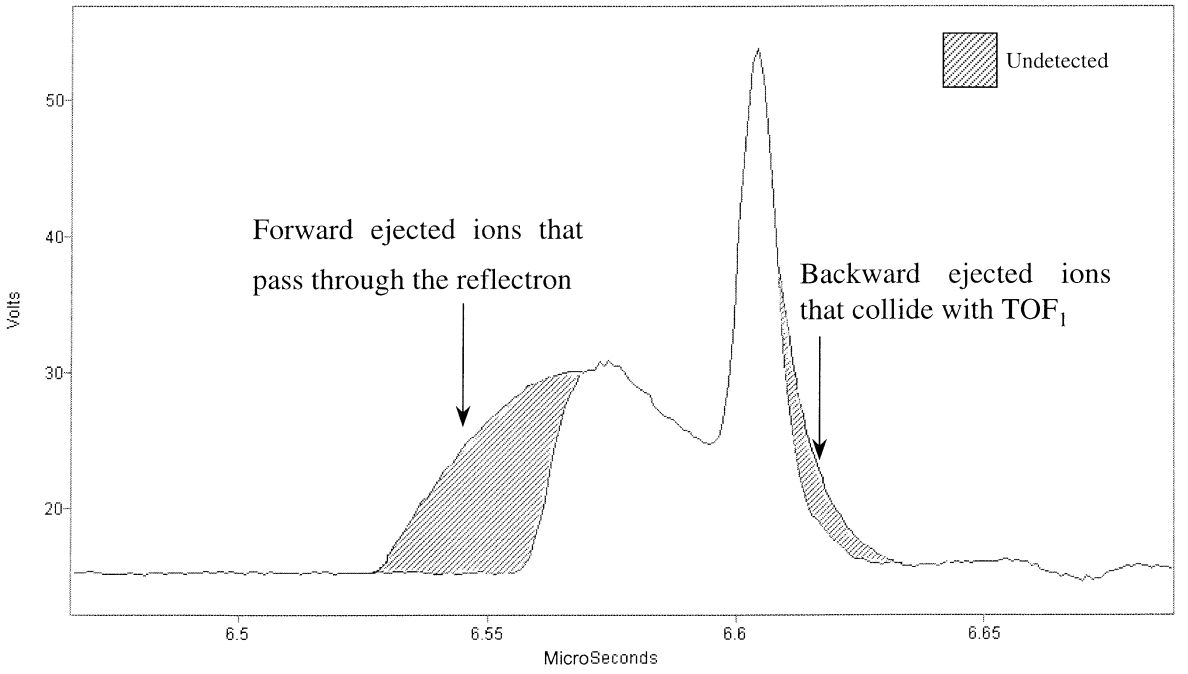

Fig. 4. This mass spectrum illustrates the forward- (broad hump) and backward-ejected (sharp peak) fragments imaged after a Coulomb explosion event. Because of the limitations of a traditional time-of-flight mass spectrometer, some energy ranges are not detected. The shaded regions arbitrarily depict the undetected energy ranges. The undetected region at earlier times extrapolate the forward-ejected ions that possess more energy than the reflectron can turn toward the detector. The extrapolated region at later times signify those ions that possess more energy than can be successfully turned by the electric field on TOF_1, which collide with the electrostatic lens.

skimmed prior to ionization with femtosecond laser pulses, which were directed to intercept clusters located between the time-of-flight grids. The time-of-flight mass spectrometer is of Wiley–McLaren design and is shown in Fig. 1 [20]. Under typical operating conditions, the potential applied to TOF_1 is between 4 and 5 kV while the potential applied to TOF_2 is roughly 3 kV. For the studies presented in this manuscript, TOF_2 was kept constant at a potential of 2982 V and the potential of TOF_1 was systematically varied while the reflectron acted as an ion mirror for ions of a prescribed energy range. Typically, the reflectron voltage is kept at a potential equal to, or higher than the potential applied to TOF_1, however, for these studies presented here, the reflectron was set to a specific value based on the potential of TOF_2. Those specific values for the reflectron are discussed below. Those ions with kinetic energy less than the potential of the reflectron are turned toward the detector while those of greater energy are not. With the potential applied to the front of the reflectron, the total flight path for the detected ions is 2 m. The detection scheme employs a pair of microchannel plates (MCPs) coupled to an oscilloscope (Agilent Technologies 54820A).

Ionization and Coulomb explosion was achieved with an amplified colliding pulse mode locked ring dye laser. In this arrangement, a gain jet containing rhodamine 590 tetrafluoroborate is pumped by a continuous wave argon ion laser (Coherent Innova 305). Continuous wave lasing from the gain jet is interrupted by a saturable absorber jet containing DODCI. Laser pulses on the order of 100 fs are generated at 90 MHz with pulse energies of only ~200 pJ. Amplification of the laser pulses is achieved in four stages using a six-pass bowtie amplifier and three successive Bethune cells where the beam is progressively expanded from a 2 mm initial diameter

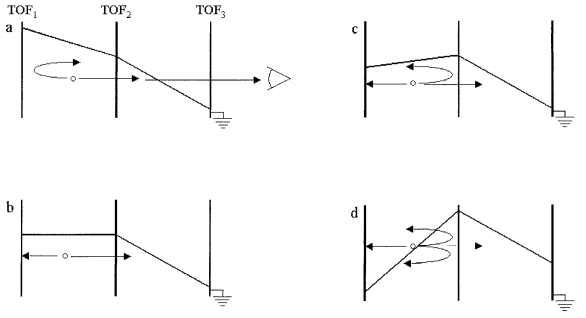

Fig. 5. (a) Typical TOF settings for the detection of cations. TOF_1 is placed at a higher positive potential than TOF_2. (b) The potential on TOF_1 is lowered to equal the potential on TOF_2 resulting in zero voltage gradient. Only ions with some kinetic energy can be detected by the TOFMS. (c) As TOF_1 is lowered further, the gradient reverses so zero and low kinetic energy cations are accelerated away from the detector. Only those ions with enough kinetic energy to climb the gradient will reach TOF_2 and be accelerated toward the detector. (d) The potential on TOF_1 can be adjusted to negative values to steepen the gradient. In this arrangement, most of the cations are accelerated away from the detector. Only those ions with a considerable amount of kinetic energy will reach TOF_2 and be accelerated toward the detector.

to a final beam diameter of 12 mm. All amplification is achieved by transverse pumping of sulphorhodamine 640 by the second harmonic of a 10 Hz Nd: yttrium-aluminum-garnet laser (Spectra Physics GCR-4). Recompression is performed using a prism pair to compensate for group velocity dispersion. The amplified laser pulse is 120–150 fs in duration, 1.0–1.5 mJ of energy and has a wavelength centered at 620 nm. The laser is focused into the mass spectrometer with a 40 cm optical lens to yield a final focused beam diameter of ~6.6 μm with peak powers of $\sim 10^{16}$ W/cm^2.

3. Results and Discussion

A determination of the kinetic energy released from Coulomb explosion events generated in water clusters was achieved using a new method called TOF gating. In the usual TOF mass spectrometer configuration situated for the detection of cations, TOF_1 is placed at a positive potential higher than that of TOF_2 and a grounding grid is located before the field free region; see Fig. 5(a). This allows all cations to be accelerated towards the reflectron and then to ultimately impact on the detector. Those ions that have energy less than the repelling grid of the reflectron are detected, while those ions with higher energy than the reflectron maintain a straight trajectory and are not imaged. TOF gating employs a method whereby the potential placed on TOF_1 is reduced while all other potentials (TOF_2, the ground potential applied to TOF_3, as well as the reflectron and MCPs) remain constant. As TOF_1 is reduced, a situation arises where the potentials are equal on both TOF_1 and TOF_2 [see Fig. 5(b)]. As shown in Fig. 5(c), eventually, the potential applied to TOF_1 becomes lower than that of TOF_2, producing a field in the opposite direction than necessary for detecting cations in the traditional method. By reversing the polarity of TOF_1 and generating a negative potential, the gradient between TOF_1 and TOF_2 can be strongly attractive, actually exceeding in magnitude the field strength between TOF_2 (2982 V) and ground; see Fig. 5(d). As the time-of-flight potential becomes more repulsive for cations, the electrons ejected from photoionization/Coulomb explosion are accelerated toward the reflectron. Because of this, experiments were performed which ruled out the possibility that cations were being generated by energetic electrons. A magnetic field was externally applied near the electrostatic lenses to deflect any electrons that might become accelerated due to the reverse gradient, and thereby possibly contribute to the birth of atomic ions in other regions of the apparatus. Mass spectra obtained in this fashion did not exhibit any change in ion intensities, determinations of ion birth potentials, or kinetic energies.

Using typical time-of-flight settings (TOF_1 = 4600 V, TOF_2 = 2982 V) with the reflectron operating as an ion mirror, a cutoff study was performed to determine the birth potential (BP) of the ions. Once the BP was determined, the distance between TOF_2 and the laser/molecule interaction region was calculated as

$$d = l\left(\frac{BP - TOF_2}{TOF_1 - TOF_2}\right) \quad (1)$$

where d is the distance of the birth location from TOF_2 and l is the total distance between TOF_1 and

TOF_2. In the present study, the distance between the grids is 1 cm and the birth location, *d*, was 0.363 cm from TOF_2. TOF gating was carried out by stepping down the voltage of TOF_1 by increments of 100 V. Eventually, when TOF_1 is at a lower potential than TOF_2, ions must overcome a positive field gradient in order to be detected. The positive field gradient was determined as

$$\left| qd \frac{(TOF_1 - TOF_2)}{l} \right| = MEKER \quad (2)$$

where *q* is the integer charge on the ion and MEKER is the minimum excess kinetic energy required for an ion to be detected. This value corresponds to the KER of the forward ejected ions from the Coulomb explosion. The reflectron was set at a constant potential, U_k, which is determined by

$$\left(\frac{d}{l} V_{Inc}\right) + TOF_2 = U_k \quad (3)$$

where V_{Inc} is the step size by which TOF_1 is decreased and U_k is the voltage on the reflectron. If one subtracts TOF_2 from U_k, the voltage window of the energetic species is obtained. In these studies, a voltage window of 36 V was utilized.

When the electric field between TOF_1 and TOF_2 diminishes to zero as in Fig. 5(b), only ions that have additional kinetic energy towards the reflectron are detected. As the potential on TOF_1 is dropped further, the minimum kinetic energy required for an ion to overcome the barrier and be detected is increased. For instance, if an ion was born between a TOF_1 grid at a potential of 10 V and a TOF_2 grid at a potential of 20 V, the ion would need excess kinetic energy equivalent to more than 5 V to make it to TOF_2 before being accelerated to ground potential and hence toward the reflectron. With any smaller energy release, the ion would be accelerated toward TOF_1 and would not be detected. In this example, if the reflectron was at a potential of 25 V, then only ions with at least 5 V but no more than 10 V would be detected. This is because an ion with 5 V would just make it to TOF_2 and be accelerated as if it only had 20 V. If that ion had 10 V, it would arrive at TOF_2 with 5 V of excess energy and be accelerated with a total of 25 V, the limit of the potential applied to the reflectron in this example. Species with higher energies would maintain a straight trajectory and not get detected.

Water clusters were generated as described above to yield mass spectra such as the one shown in Fig. 6. Protonated water clusters are observed for sizes of $H^+(H_2O)_n$, $n \leq 21$, though larger clusters may fragment and remain undetected. At larger cluster sizes, metastable decay can be seen as secondary peaks at shorter arrival times. These daughter peaks arise from evaporation of a parent peak in the field free region. A blown up region can be seen in the inset of Fig. 6 where multicharged oxygen atoms arrive. Fig. 7 represents a mass spectrum of water where little clustering is present, and the unprotonated monomer of water is dominant. As can be seen, in the absence of large water clusters very little multicharging is observed for oxygen. The singly and doubly charged carbon atoms arise from diffusion pump oil.

Fig. 8 illustrates the distribution of protons detected at various MEKER values. The abscissa contains the MEKER for an ion to escape the attractive potential gradient and be detected. MEKER values were calculated previously by equation 2. The ordinate of Fig. 8 is the percentage of ions with a particular KER range. The inset graph in Fig. 8 is from the same data set, but is rescaled to illustrate the behavior of the proton at various selected values. The scales are expanded to display features in the data where very little intensity arises at a particular range of kinetic energy release, and to also demonstrate that real signal above background ion signal is being measured at the various respective MEKER values.

Three distinct regions can be seen in the MEKER plot for protons. The first region is where there is a steep drop-off just beyond zero MEKER. This illustrates that the ejected protons have the highest probability of having kinetic energies of less than 100 V arising from a Coulomb explosion event. The second region of interest shows a relatively smooth reduction of probability to a value of ~2000 V kinetic energy. Finally, the third region shows a slight increase in MEKER and remains elevated to the limits of our experimental apparatus at 3300 V. The average ki-

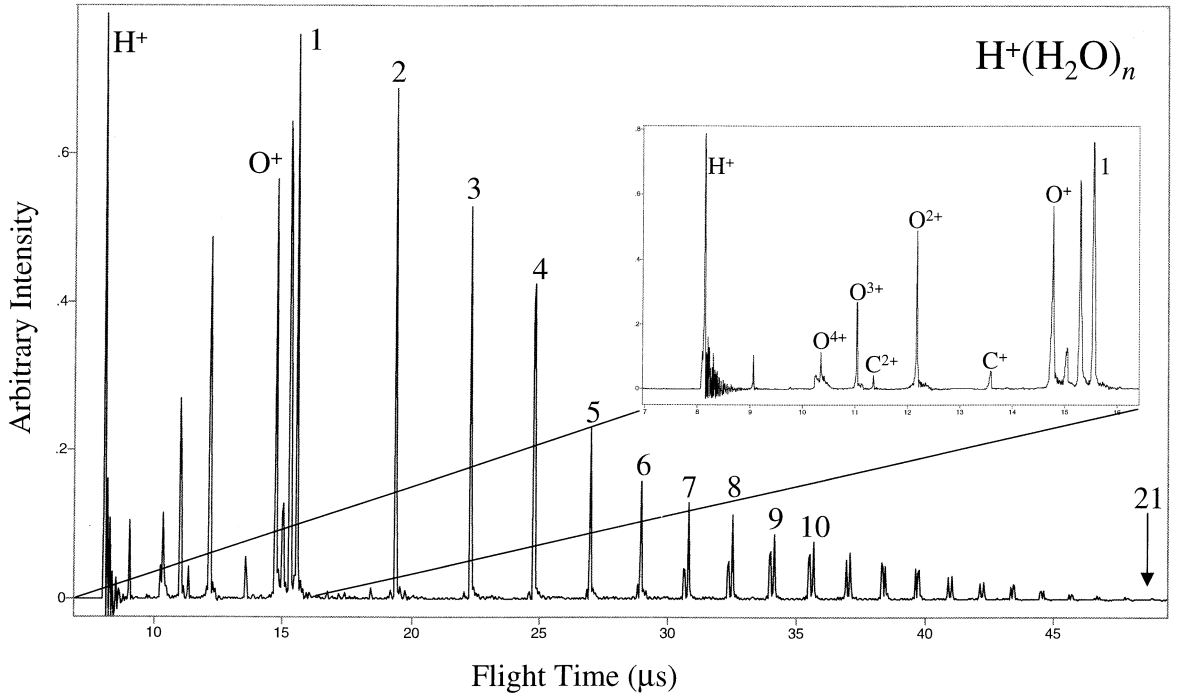

Fig. 6. A mass spectrum of water clusters obtained with the TOFMS at typical voltage settings. The inset illustrates the low *m/z* range where multicharged ions are evident. The sharp cutoff on the left side of the O^{4+} results from a loss of high-energy fragments that maintain a straight trajectory through the reflectron and fail to be detected. Those peaks that arrive at slightly shorter flight times next to the protonated water clusters are a result of metastable decay and represent the loss of one water molecule.

netic energy release ⟨KER⟩ determined from the percentage plots for the proton is 387 V and was calculated with

$$\langle KER \rangle = \sum_i \left((MEKER)_i \frac{I_i}{\sum_i I_i} \right) \quad (4)$$

where I_i is the peak area associated for a particular MEKER value. This average kinetic energy release is similar to the findings from Poth's simulation for the 19-mer of acetone.[7] In this study, Poth found that the protons resulting from Coulomb explosion of the acetone cluster yield a distribution of kinetic energies around 800 eV. While Poth's study does not directly compare to the water case, the calculated average kinetic energy of ejected protons being ∼387 eV seems very plausible.

The MEKER plots for O^+ display a sharp drop off to ∼100 V, followed by a long decay to ∼3000 V; it is likely that the energy distribution extends beyond this magnitude (see Fig. 9). The MEKER plots for the O^{2+} and O^{3+} (Figs. 10 and 11) show interesting behavior. It is important to note that each of these MEKER plots (O^+, O^{2+}, O^{3+}, and O^{4+}) come from the same data set, however, the abscissa is modified for each plot due to the different range of kinetic energies that each of the multicharged atoms acquires in the Coulomb explosion process resulting from the individual charge state on each atom. The O^{2+} MEKER plot shows an even drop off in intensity to a value of around 400 V. The O^{2+} exhibits nonzero probabilities around 2400, 3800, and 5000 V. The O^{3+} ion drops off quickly to ∼400 V, but displays a local maximum of probability in the regions of 3500 and 7200 V.

The O^{4+} cation MEKER plots are given in Fig. 12. It is of particular interest to mention that the first MEKER voltage of 72±72 V yielded no ion signal. Since the O^{4+} cation generated from a Coulomb

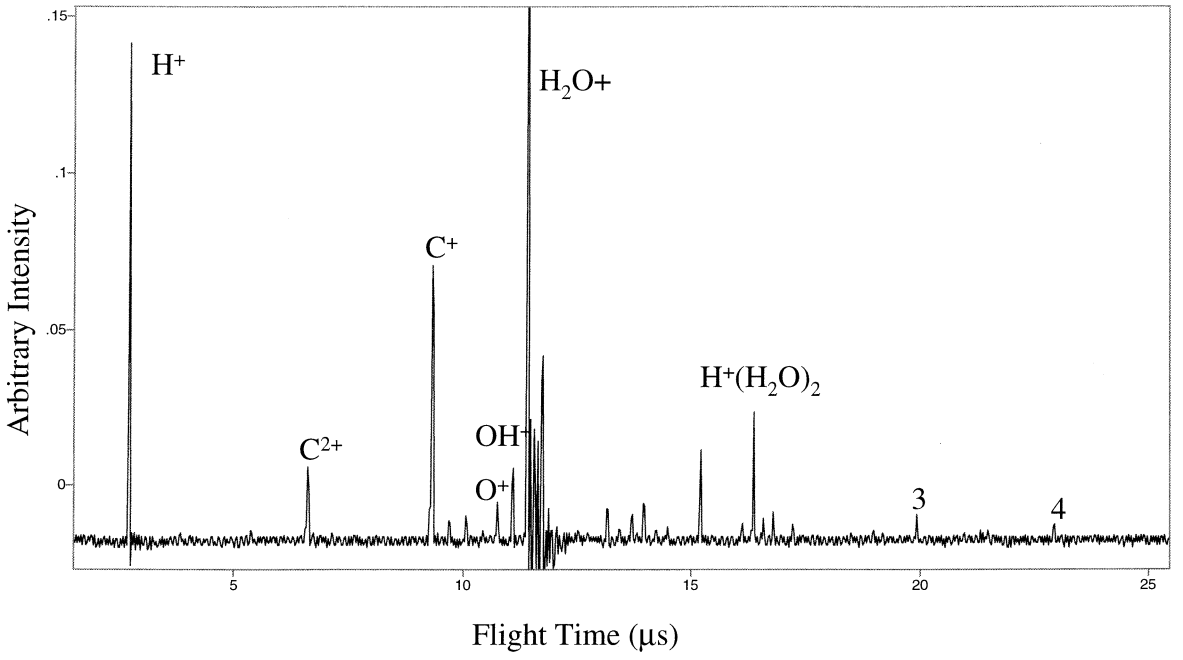

Fig. 7. A mass spectrum of water where expansion conditions were modified to eliminate a majority of the larger clusters. Here, a minor intensity can be attributed to the $H^+(H_2O)_4$ cluster. The carbon species observed in the mass spectrum are due to the ionization of diffusion pump oil.

explosion event does not indicate an ion signal at these low MEKER values, this suggests that the generation of these species must come from clusters that are able to impart a large fraction of their Coulomb potential to an O^{4+} cation. The Coulomb potential increases greatly with cluster size as ions in close proximity repel each other more forcefully as the density of atoms increases. A short discussion of the Coulomb potential of the water monomer and dimer is given below.

No particular range of kinetic energy release dominates the series of the O^{4+} MEKER. The most probable energy range exhibited from the MEKER plot exists around 1000 V and only comprises 4.5% of the total energy range detected. The O^{4+} MEKER plot exhibits two very distinct local maxima around 1000 and 4500 V. Two other local maxima can be seen around 6300 and 9500 V, but these are not so apparent. The O^{4+} signal slowly reduces to a value of approximately 0.1% for the highest energy range of ~13 keV. The kinetic energy release would likely extend further, but the experiments were performed to the limits of the potentials that can be applied to our TOFMS.

While the energy release for the O^{4+} seems quite large, it is not improbable that a large water cluster could produce enormous kinetic energy release. Based on a molecular dynamics simulation of acetone clusters, Poth et al. reported a maximum kinetic energy release values for oxygen being 4400 eV. Simulations performed on the acetone cluster (n = 19) with assigned charges of +2 for the oxygen and +4 for the carbon, yielded maximum values of 1800 V for O^{2+} and 2400 V for C^{4+}. From these theoretical calculations, it seems possible that an O^{4+} ion can have significant kinetic energy release. Poth's calculations also show there are regions that have zero probabilities for certain KER; a similar finding is observed in these experiments for the O^{2+} and O^{3+} MEKER plots. Coulomb explosion of a single cluster size yields discrete energy values. These discrete energy values become obscured in these studies since

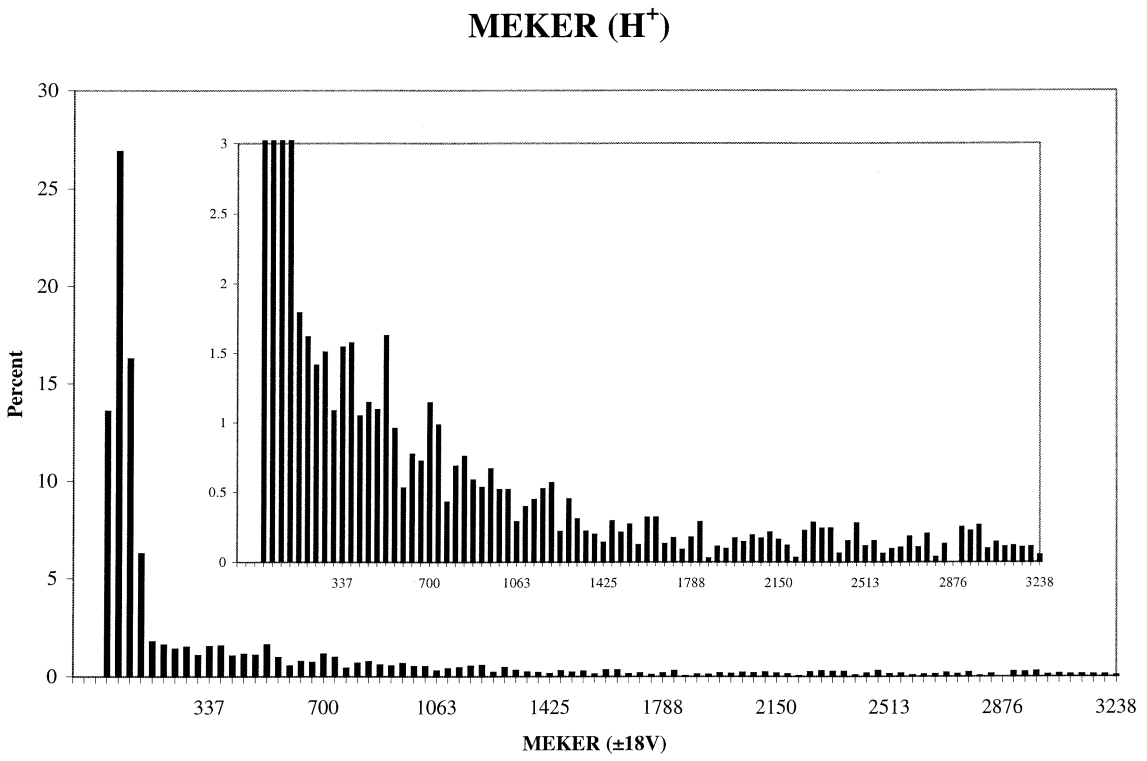

Fig. 8. MEKER plot for the proton. More than 75% of the protons generated from Coulomb explosion in these studies have excess kinetic energies in a range between 0 and 150 V.

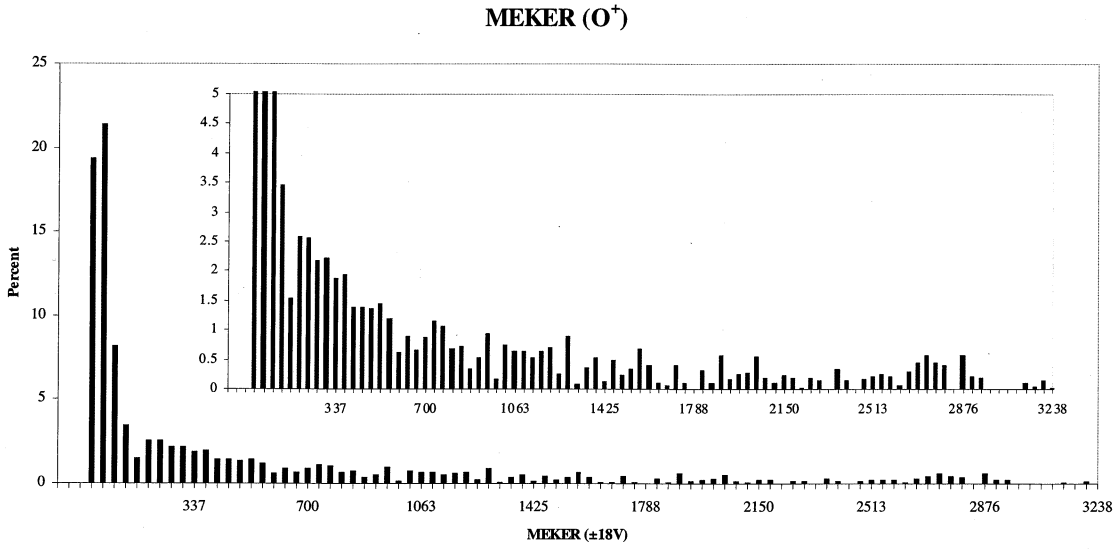

Fig. 9. MEKER plot for O^+. The voltage window employed for this ion was 36 V (18±18 V).

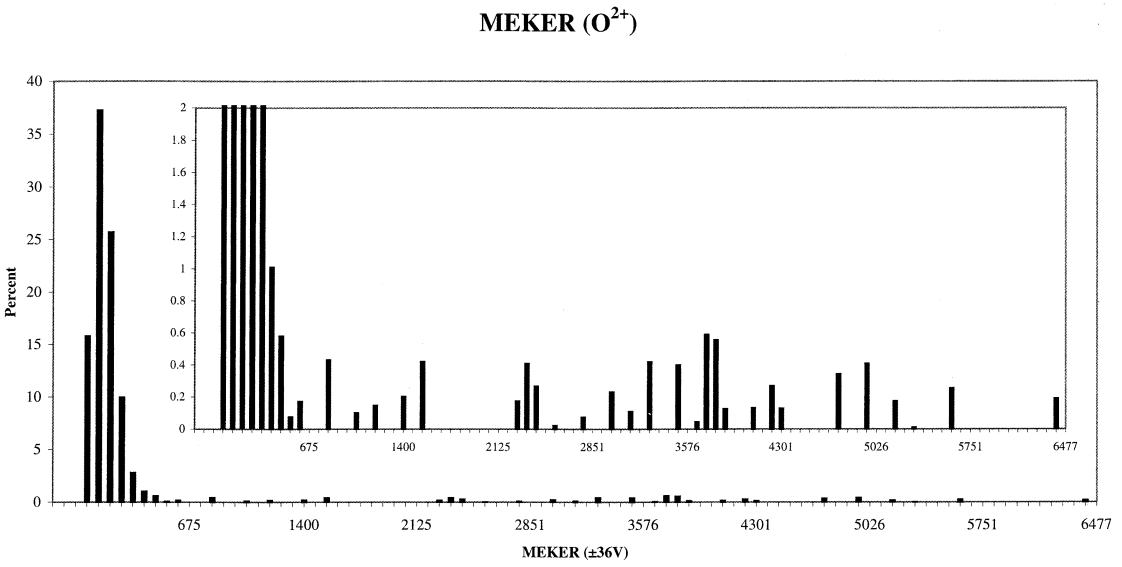

Fig. 10. MEKER plot for O^{2+}. The voltage window for the O^{2+} ion was 36±36 V since the doubly charged ion feels an electric field twice as strong as the singly charged oxygen atom.

an entire distribution of water clusters is simultaneously imaged. It seems likely that some of the discrete energy spacing would still be detectable in our experiments. Plans for future studies include study of the Coulomb explosion of a single cluster size, which could be directly correlated with simulations of particular clusters.

Furthermore, TOF gating was performed for mass spectrometric distributions that contained only water monomer and a minor amount of small water clusters.

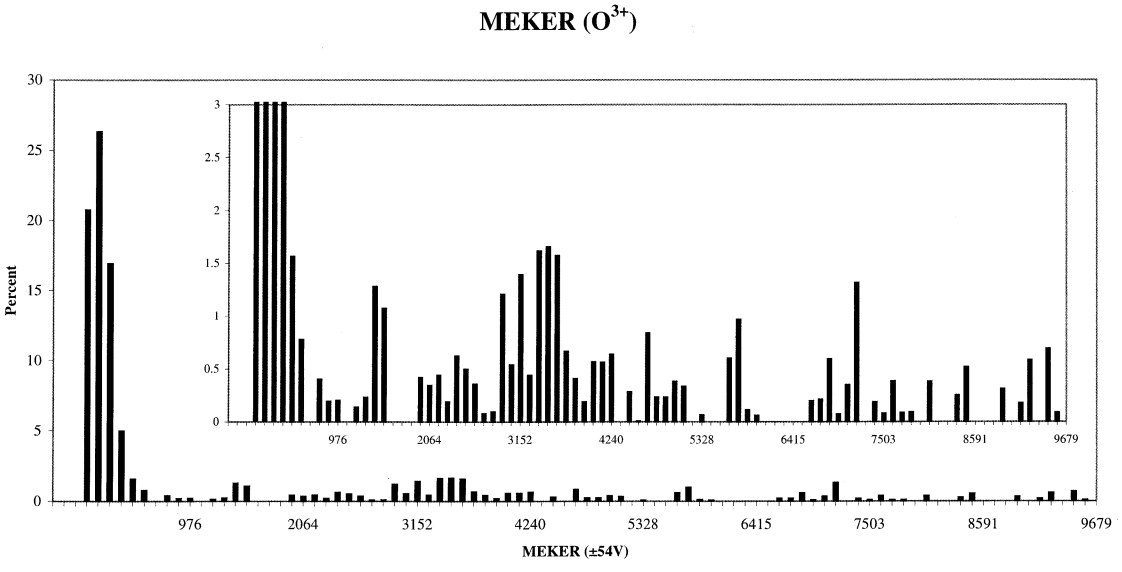

Fig. 11. MEKER plot for O^{3+}. The voltage window was 54 ±54 V.

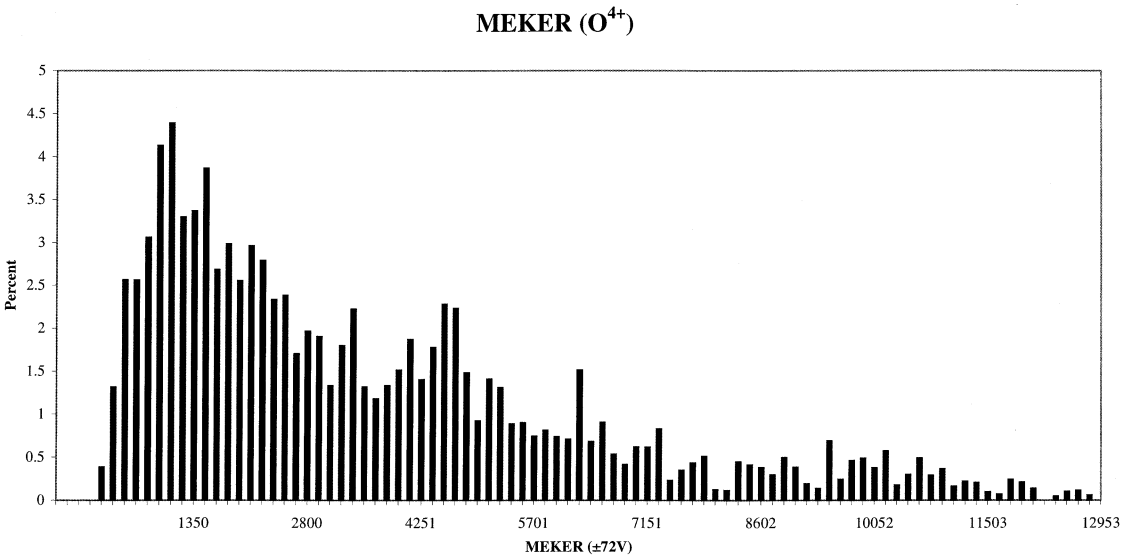

Fig. 12. MEKER plot for O^{4+}. The voltage window for the O^{4+} ion was 72±72 V.

This was achieved both by reducing the backing pressure of the carrier gas and by reducing the time the pulse nozzle was open that allows water vapor seeded in helium to enter the vacuum of the mass spectrometer (see Fig. 7). A MEKER plot was calculated for the proton in this experimental situation and is given in Fig. 13. As can be seen from the plot, peaks with high energy were not detected and the

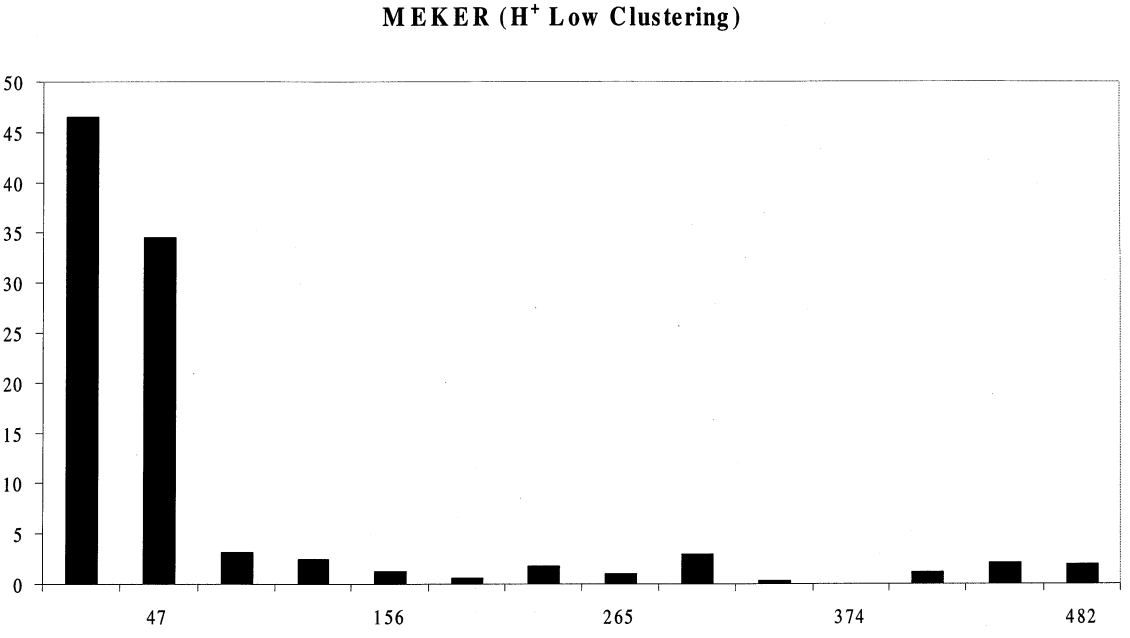

Fig. 13. MEKER plot for H^+. As the amount of clustering is reduced, the kinetic energy release is lowered.

Table 1
Comparisons of the average kinetic energy released determined from MEKER plots for two expansion conditions; when large clusters are present, the proton average KER is much larger than when only low order clusters are present

Average KER from Differing Cluster Conditions			
Ion	$H^+ (H_2O)_{n=1–20}$	$H^+ (H_2O)_{n=1–4}$	
H^+	387	74	V

average kinetic energy release was significantly lower than for the high order cluster case. Table 1 shows the calculated kinetic energy release for the proton in the two cases. Some of the protons detected in the mass spectrum are due to the hydrocarbon pump oil. However, as evidenced by the ion signal corresponding to O^+ and OH^+, the proton signal acquires significant contribution from fragmented water and water clusters.

Calculations of the Coulomb potential made for water monomer during the course of this study with oxygen in the +4 state yielded a maximum energy release of 130 V. A similar calculation was performed for the dimer species, which determined a Coulomb potential of 430 V [21]. These values were determined from calculations utilizing

$$V = \frac{1}{4\pi\varepsilon_0} \sum_{i \neq j} \frac{q_i q_j}{r_{ij}} \tag{5}$$

where ϵ_0 is the vacuum permittivity constant, q_i is the charge on ion i and r_{ij} is the distance between ions i and j. Calculations of the Coulomb potential for larger clusters become increasing complex, so only the monomer and dimer were considered thus far. The maximum energy (by percent) detected for the proton was less than 100 V (~9%) with other values for the proton kinetic energy release being up to 500 V (<1%). The maximum values of kinetic energy release calculated from the Coulomb potentials agree well with the energy values obtained from the MEKER plots.

Comparisons were drawn between the TOF gating study and the peak splitting method developed in our laboratory. The peak splitting method calculates the average kinetic energy release employing

$$KER = \frac{q^2 \Delta t^2}{8m} \left(\frac{TOF_1 - TOF_2}{l} \right)^2 \tag{6}$$

where q is the integer charge of the ion multiplied by the fundamental charge of an electron (C), Δt is the time between the forward and backward peaks (s), m is the mass of the ion (kg), TOF_1-TOF_2 is the potential (V), and l is the distance between the grids (m). From this method, the average kinetic energy release for the proton peak was determined to be 108 eV. This was determined from an individual mass spectrum where many water clusters were present.

This value seems low in comparison with what is reported here based on the TOF gating experiments. The TOF gating experiments, however, allow very high-energy species to be detected that would normally pass through the reflectron and would not be detected in typical studies. For instance, if an ion with 3000 V kinetic energy release was fired forward with an initial birth potential of 3500 V, the reflectron would need to be greater than 6500 V to successfully turn the ion around toward the detector and be imaged. However, in the TOF gating experiments, if the same ion was created with an effective birth potential of −2900 V, then the ion would have an initial kinetic energy of 100 V before being accelerated by TOF_2. With this method, an ion with 3000 V of kinetic energy would be detected as if it possessed only 100 V of kinetic energy release. This new kinetic energy analysis method allows a broader range of high-energy ions to be detected and KER values to be determined more easily.

The theory necessary in developing the cutoff and peak splitting methods is correct but, unfortunately, considerable data can be lost due to the limitations of the typical TOF mass spectrometer. The full distribution of the forward- and backward-ejected ions can become truncated so that only the lower energy species are detected; this would lead to a biased lower value for the determined average kinetic energy release than is the physical case (refer to Fig. 4). Table 2 illustrates the average kinetic energy calculated by several different methods. As can be seen, the peak splitting method revealed an average kinetic energy release of 108 V for the proton. By truncating the

Table 2
Kinetic energy release was determined by several methods; peak splitting revealed an average KER of 108 V from a mass spectrum obtained at the TOFMS values listed; MEKER plots resulted in an average KER of 387 V; however, adjusting the MEKER plots to truncate protons with energies too great to be reflected (> 370 V) resulted in an average KER of 102 V; theoretical values of the KER were also determined from the calculated time of arrival (CTA) for the two peaks

Calculated Average Kinetic Energy Values				
Method	H^+ KER (V)	TOF_1 (V)	TOF_2 (V)	U_k (V)
Peak splitting	108	3400	2982	3500
Adjusted MEKER	102	Variable	2982	3018
MEKER	387	Variable	2982	3018
ΔCTAs	110	3400	2982	3500

MEKER plot for the proton at the maximum energy value that could be detected in a typical TOF setup, an average kinetic energy release was determined to be 102 V. Truncation was performed by first determining the maximum kinetic energy release detectable from the mass spectrum that yielded the average kinetic energy release determined by peak splitting. A value of 370 V could be detected for the proton. By ignoring those kinetic energy values higher than this maximum detectable range (>370 V), an adjusted average kinetic energy can be obtained. This is clear evidence that employing the MEKER approach enables the determination of a more complete average kinetic energy for highly energetic species.

4. Conclusions

A new method for the detection and characterization of energetic species produced from a Coulomb explosion event is reported. The magnitude of kinetic energy release in Coulomb explosion can be beyond the scope of the electronics in a TOFMS when operating under typical settings. The TOF gating method removes the low or zero kinetic energy ions and slows high-energy ions in a controlled manner for facile detection. Kinetic energy release values for O^{4+} of greater than 13 kV were reported here arising from water clusters. Maximum proton kinetic energy release was determined to be greater than 3 kV. Furthermore, comparisons of the TOF gating study have been made with previous methods for determining kinetic energy release, the cutoff and the peak splitting methods. The average kinetic energies determined from these methods are actually the average kinetic energy of the detected species. The high-energy species are lost either by collision with the TOF_1 plate (backwards ejected ions) or by passing through the reflectron (forward ejected ions).

The oxygen MEKER plots (Figs. 9–12) reveal possible clues to solvation shells of water clusters as well as the location of high charge states within a cluster that undergoes Coulomb explosion. The MEKER plots for O^{2+} and O^{3+} illustrate several regions having zero probability, with the plots being dominated by probabilities of lower energy release. This dominance by lower energy species is suggestive that ions with lower charge states either are born in clusters that do not develop high charge states or may reside in the middle regions of the cluster where they are less likely to garner significant kinetic energy. The O^{4+} plots have several local maxima that may be indicative of solvation shells. As the water clusters grow in size to accommodate additional layers, the energy available to outer ions from a Coulomb explosion event would increase to perhaps yield well-defined energy regions. Theoretical computations of large cluster systems are necessary to help resolve these possibilities.

Acknowledgement

The authors would like to thank AFOSR, Grant No. F49620-01-1-0122, for the financial support of this research.

References

[1] S. Wei, J. Purnell, S.A. Buzza, E.M. Snyder, A.W. Castleman, Jr., in Femtosecond Chemistry, J. Manz and L. Wöste (Eds.), Springer-Verlag, Germany, 1994, p. 449.
[2] S.A. Buzza, E.M. Snyder, D.A. Card, D.E. Folmer, A.W. Castleman, Jr., J. Chem. Phys. 105 (1996) 7425.
[3] J. Purnell, E.M. Snyder, S. Wei, A.W. Castleman, Jr., Chem. Phys. Lett. 229 (1994) 333.
[4] T.D. Ditmire, J. Zweiback, V.P. Yanovsky, T.E. Cowan, G. Hays, K.B. Wharton, Phys. Plasmas 7 (2000) 1993.
[5] J.V. Ford, Q. Zhong, L. Poth, A.W. Castleman, Jr., J. Chem. Phys. 110 (1999) 6257.
[6] M. Lezius, S. Dobosz, D. Normand, M. Schmidt, Phys.Rev. Lett. 80 (1998) 261.
[7] L. Poth, A.W. Castleman, Jr., J. Phys. Chem. 102 (1998) 4075.
[8] T. Ditmire, J. Zweiback, V.P. Yanovsky, T.E. Cowan, G. Hays, K.B. Wharton, Phys. Plasmas 7 (2000) 1993.
[9] E.M. Snyder, S.A. Buzza, A.W. Castleman, Jr., Phys. Rev. Lett. 77 (1996) 3347.
[10] E.M. Snyder, S. Wei, J. Purnell, S.A. Buzza, A.W. Castleman, Jr., Chem. Phys. Lett. 248 (1996) 1.
[11] K. Boyer, T.S. Luk, J.C. Solem, C.K. Rhodes, Phys. Rev. A 39 (1989) 1186.
[12] D.E. Folmer, L. Poth, E.S. Wisniewski, A.W. Castleman, Jr., Chem. Phys. Lett. 287 (1998) 1.
[13] K. Boyer, B.D. Thompson, A. McPherson, C.K. Rhodes, J. Phys. B: At. Mol. Opt. Phys. 27 (1994) 4373.
[14] C. Rose-Petruck, K.J. Schafer, C.P.J. Barty, in Applications of Plasma Radiation II, M.C. Richardson, G.A. Kyrala (Eds.), SPIE, Bellingham, 1995, Vol. 2523, p. 272.
[15] T. Zuo, A.D. Bandrauk, Phys. Rev. A 52 (1995) 1.
[16] I. Last, J. Jortner, Phys. Rev. A 58 (1998) 3826.
[17] T. Seideman, M.Y. Ivanov, P.B. Corkum, Phys. Rev. Lett. 75 (1995) 2819.
[18] D. Card, D.E. Folmer, E.S. Wisniewski, A.W. Castleman, Jr., unpublished.
[19] J.V. Ford, L. Poth, Q. Zhong, A.W. Castleman, Jr., Int. J. Mass. Spectrom. 192 (1999) 327.
[20] W.C. Wiley, I.H. McLaren, Rev. Sci. Instrum. 26 (1956) 1150. [21] R.N. Barnett, U. Landman, J. Phys. Chem. 99 (1995) 17305.